ResearchGate

See discussions, stats, and author profiles for this publication at: https://www.researchgate.net/publication/230525825

Effect of block molecular weight distribution on the structure formation in block copolymer/homopolymer blends

ARTICLE *in* JOURNAL OF POLYMER SCIENCE PART B POLYMER PHYSICS · JANUARY 2012

Impact Factor: 3.83 · DOI: 10.1002/polb.22339

CITATIONS
7

READS
22

6 AUTHORS, INCLUDING:

Jessica Listak

8 PUBLICATIONS **187** CITATIONS

SEE PROFILE

Andrzej Plichta

Warsaw University of Technology

20 PUBLICATIONS **164** CITATIONS

SEE PROFILE

Mingjiang Zhong

Massachusetts Institute of Technology

42 PUBLICATIONS **930** CITATIONS

SEE PROFILE

Michael R Bockstaller

Carnegie Mellon University

92 PUBLICATIONS **2,249** CITATIONS

SEE PROFILE

Available from: Michael R Bockstaller
Retrieved on: 17 January 2016

Effect of Symmetry of Molecular Weight Distribution in Block Copolymers on Formation of "Metastable" Morphologies

Jessica Listak,[†] Wojciech Jakubowski,[‡] Laura Mueller,[‡] Andrzej Plichta,[‡] Krzysztof Matyjaszewski,*[,‡] and Michael R. Bockstaller*[,†]

Department of Materials Science and Engineering, Carnegie Mellon University, 5000 Forbes Ave., Pittsburgh, Pennsylvania 15213, and Department of Chemistry, Carnegie Mellon University, 4400 Fifth Ave., Pittsburgh, Pennsylvania 15213

Received September 6, 2007

ABSTRACT: Polystyrene-*b*-poly(methyl acrylate) (PS−PMA) copolymers were synthesized using activators regenerated by electron transfer (ARGET) for atom transfer radical polymerization (ATRP). Polydispersity of the PMA block was varied by adjusting the amount of copper catalyst in ARGET ATRP, and the resulting molecular weight distributions were found to be approximately symmetric. At a composition of 35 vol % of PMA, the formation of a hexagonally perforated lamellar (*HPL*) morphology was observed for a polydisperse PS−PMA copolymer for short- and long-term solvent-casting conditions. No order−order transitions were observed at elevated temperatures or after prolonged thermal annealing. The observed stabilization of the *HPL* morphology—that is considered to be metastable in narrow-disperse diblock copolymers as well as diblock copolymers with selective block polydispersity given by a Schulz−Zimm distribution—suggests that the skewness of the distribution of block molecular weights is an important parameter for the structure selection during the microphase separation process. In particular, the results indicate that near-symmetric block molecular weight distributions (as realized by the ARGET ATRP technique) facilitate the stabilization of microdomain morphologies with increased standard deviation of mean curvature. The results point to the relevance of controlling both the width *and* symmetry of molecular weight distribution as a potential route toward the tailored synthesis of nonregular microstructures with particular topological properties that might be of future technological interest.

Introduction

The ability of block copolymers (BCP) to autonomously organize into periodic microdomain structures that combine the characteristics of periodic nanostructures with the chemical functionality imparted by the composition of the respective blocks has led to exciting opportunities for block copolymer-based materials in new areas of technology.[1,2] The further development of this promise will depend on the ability to expand the range of accessible block chemistries and—ideally—morphologies that can be realized with block copolymers. Controlled/living radical polymerization (CRP) methodology, which was developed in the mid-1990s, can be applied to the preparation of many different well-defined (co)polymers.[3] Techniques such as atom transfer radical polymerization (ATRP),[4−6] nitroxide-mediated polymerization (NMP),[7] or reversible addition−fragmentation chain transfer (RAFT)[8] allow the preparation of polymers with predetermined molecular weights, low polydispersity, controlled composition, and topology. Because radical polymerization is very tolerant of functional groups, a broad range of unsaturated molecules can be polymerized. Recent advances in the field of controlled radical polymerization (ARGET ATRP, see below) present a further breakthrough that expands the possibilities to tailor the characteristics of BCP by facilitating precise control of the block molecular weight distribution or polydispersity index (PDI).

Theoretically, the effect of polydispersity on BCP phase behavior was first studied by Leibler et al., who suggested that chain length disparity results in increased compositional fluctuations.[9] Later, Hong et al. and Burger et al. predicted polydispersity in BCP to result in increased domain spacing of the ordered state and a decrease of the critical degree of segregation $(\chi N)_{crit}$.[10,11] Self-consistent-field simulations (SCFT) confirm these prior predictions and suggest that block-selective polydispersity (i.e., BCP with mono- and polydisperse blocks) results in the stabilization of topological defects as well as the shift of the stability regions of the various morphologies.[12−14] In particular, Sides and Fredrickson demonstrated a cylinder (*C*) to sphere (*S*) transition for a diblock copolymer at fixed average volume composition ($\phi = 0.3$) and degree of segregation ($\chi N = 18$) as the polydispersity index (PDI) of the minority block was increased from PDI = 1 to 1.5.[12] By evaluating the grand-canonical free energy using SCFT, Matsen recently predicted the formation of $L + C$ coexistence regions through fractionation of the molecular weights. These two-phase regions were observed to widen with increasing PDI and to effectively constrain the stability region of the gyroid (*G*) phase.[15]

Because of the difficulties of combining continuous polydispersity with control of the average molecular weight in the synthesis of BCP, most experimental research on the effect of polydispersity on BCP self-assembly has focused on bi- and multimodal blends of narrow-disperse BCP.[16−21] In these studies, the effect of segment distribution on the BCP self-assembly was found to correlate well with the theoretical predictions. In particular, it could be demonstrated that the "cosurfactant effect" of the low-molecular-weight component can be used to control the interfacial curvature in the blend microstructure.[18,19] However, as the chain length disparity increases, the blend compositions were found to undergo macrophase separation.[20,21] This is in contrast to studies on polydisperse block copolymers with continuous molecular weight distributions. In early studies, Hashimoto and co-workers reported the polydispersity of polystyrene-*b*-polyisoprene copolymers to have only minor influence on the regularity of the resulting microdomain structures.[22] Later, Bendejacq et al. demonstrated a high degree of order in polydisperse polystyrene-*b*-poly(acrylic acid) copolymers with PDI = 1.73.[23] More recently, Lynd et al.

* Corresponding authors: e-mail km3b@andrew.cmu.edu, Ph 412 268 3209, Fax 412 268-6897 (K.M.); e-mail Bockstaller@cmu.edu, Ph 412 268 2709, Fax 412 268 7247 (M.R.B.).
† Department of Materials Science and Engineering.
‡ Department of Chemistry.

10.1021/ma800816j CCC: $40.75 © 2008 American Chemical Society
Published on Web 07/02/2008

investigated the phase behavior of low-molecular-weight, asymmetric poly(ethylene-*alt*-propylene)-*b*-poly(DL-lactide) (PEP−PLA) copolymers in the strong segregation limit ($\chi N \sim 100$) consisting of a monodisperse PEP and polydisperse PLA segments.[24] This is the only report where PDI of one of the blocks was finely tuned from 1.2 to 2.0 by capitalizing on the equilibrium nature of ring-opening polymerization. Unfortunately, this method is applicable only for lactone-type monomers. Lattice disorder was found to be negligible even at high PDI, and block polydispersity was shown to induce changes in interfacial curvature depending on the weight fraction of the polydisperse component. In agreement with previous reports, the lamellar spacing was found to increase with increasing PDI. In a recent study, Ruzette et al. studied the microdomain formation of poly(methyl methacrylate)-*b*-poly(*n*-butyl acrylate) (PMMA−PBA) with slight asymmetry in the block polydispersity ($PDI_{PMMA} = 1.4-2.4$, $PDI_{PBA} = 1.2-1.9$).[25] However, typical for the applied synthetic process, PMMA blocks had high PDI and limited control of molecular weights. No macrophase separation was observed for any composition, and the stability region of the lamellar microstructure was shown to be shifted toward asymmetric compositions, in agreement with theoretical predictions.

While these previous experimental studies have generally shown qualitative agreement with theoretical predictions, it is important to note that all numerical studies to date have assumed a Schulz−Zimm distribution to represent the block molecular weight distribution. The latter is an empirical two-parameter distribution that is frequently used to describe polymerization reactions leading to positively skewed molecular weight distributions such as step-growth processes. The implication of a positively skewed molecular weight distribution is that with increasing PDI the average molecular weight is determined by an increasingly larger number of small chains and a smaller number of very large chains (see discussion below). Note that living polymerizations typically result in significantly more symmetric distributions. Since the abundance of small and large chains affects the packing frustration of chains within the microdomain structures, the symmetry of the molecular weight distribution should be an important parameter in determining the equilibrium morphology of a block copolymer. Here, we demonstrate a straightforward method for controlling the PDI in block copolymers via the recently discovered "activators regenerated by electron transfer for atom transfer radical polymerization" (ARGET ATRP), leading to a near-symmetric distribution of block molecular weights.[27] Subsequently, we demonstrate that block polydispersity within the minority domain of a polystyrene-*b*-poly(methyl acrylate) (PS−PMA) copolymer with a volume-filling fraction of PMA of $\phi_{MA} = 35\%$ stabilizes the formation of a hexagonally perforated lamellar (*HPL*) morphology that is interpreted to be a near-equilibrium (or equilibrium) state for the present system. Finally, we provide a qualitative argument to rationalize that the broad symmetric distribution of block molecular weights provides a means to stabilize morphologies that exhibit significant deviations from the average curvature of the intermaterial dividing surface.

Results and Discussion

Narrow-disperse and polydisperse PMA (abbreviated in the following as PMA_N and PMA_P, respectively) were synthesized using ARGET ATRP. This new method facilitates a decrease in the amount of catalyst needed for an ATRP from 10 000 to 10 ppm or less, by applying a reducing agent, such as tin(II) 2-ethylhexanoate (or ascorbic acid), to continuously regenerate the Cu catalyst which is otherwise consumed in termination reactions when used at very low concentrations (Scheme 1).[27–32] Lowering the concentration of the catalysts not only results in "greener" polymerization processes but also allows for the synthesis of polymers with high molecular weight and high chain-end functionality. ARGET ATRP was successfully applied to the preparation of a variety of polymeric materials including homopolymers, block and random copolymers, and development of a scalable process for preparation of molecular brushes on a flat surface.[33] Moreover, it was demonstrated that the polydispersity of homopolymers as well as individual segments in BCP can be effectively controlled by adjusting the amount of catalyst in ARGET ATRP.[34] PMA_N was synthesized using 50 ppm amount of copper catalyst ($M_n = 18\,300$ g/mol, PDI = 1.11), and PMA_P was prepared using 5 ppm amount of copper catalyst ($M_n = 18\,500$ g/mol, PDI = 1.77) (Figure 1a). The molecular weight data was measured by gel permeation chromatography (GPC) using linear PS standards for calibration.

Scheme 1. Mechanism for ARGET ATRP Reaction[a]

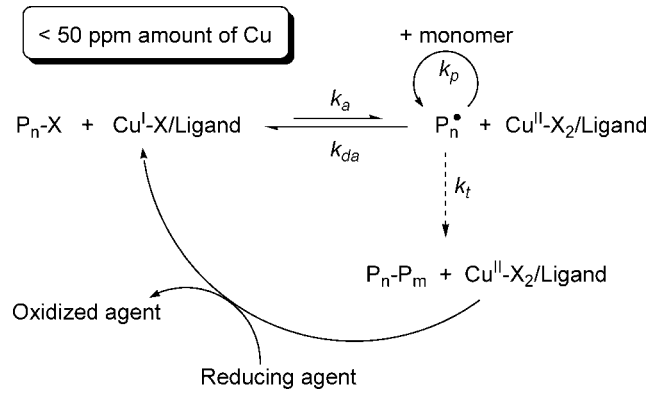

[a] This new method provides a continuous controlled polymerization with a significant reduction of the amount of copper-based catalyst complex (<50 ppm) due to a constant regeneration of the Cu(I) activator species by reducing agents, which compensate for any loss of Cu(I) by termination. By varying the amount of Cu in the system, PDI of resulting polymers can be tuned.

The conditions used to synthesize PMA_N and PMA_P were then applied to prepare the block copolymers $(PS-PMA)_{NN}$ ($M_n = 47\,200$ g/mol, PDI = 1.11, $\phi_{MA} = 0.29$) and $(PS-PMA)_{NP}$ ($M_n = 51\,700$ g/mol, PDI = 1.13, $\phi_{MA} = 0.35$) by starting from a narrow-disperse PS macroinitiator ($M_n = 31\,100$ g/mol, PDI = 1.11) and chain extending with MA using 50 ppm and 5 ppm amount of copper catalyst, respectively (Figure 1b). Although the GPC traces of both block copolymers were monomodal, liquid chromatography under critical conditions (LCCC) revealed the presence of a small amount of residual PS macroinitiator (4% for $(PS-PMA)_{NN}$ and 7% for $(PS-PMA)_{NP}$) (Figure 1c). Two-dimensional HPLC/GPC traces of these samples are available in the Supporting Information (Figure S1). The precise composition of both block copolymers was determined by ^1H NMR to be $x_{MA,NMR} = 0.35$ for $(PS–PMA)_{NN}$ and $x_{MA.NMR} = 0.43$ for $(PS–PMA)_{NP,}$ where x_i denotes the mole fraction of component i. From this data, a more precise molecular weight of the BCP could be calculated on the basis of the molecular weight of the PS macroinitiator (GPC) and the mole fraction of each block (NMR): $M_{n,NMR} = 45\,100$ g/mol for $(PS-PMA)_{NN}$ and $M_{n,NMR} = 50\,200$ g/mol for $(PS-PMA)_{NP}$.

The shapes of GPC traces shown in Figure 1a,b support the approximately symmetric shape of molecular weight distributions that is facilitated by ARGET ATRP (a more detailed discussion on the expected MWD of PMA resulting from ARGET ATRP is provided in the discussion below).[35]

PS−PMA was chosen as the model system for the present study because of the weak conformational asymmetry of PS and PMA (i.e., both polymer components exhibit comparable

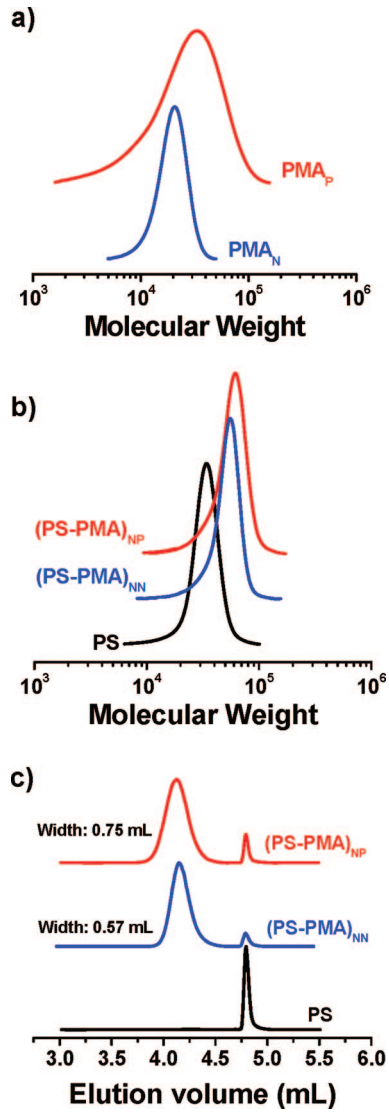

Figure 1. Panel a: GPC traces of PMA homopolymers PMA_N (ARGET ATRP with 50 ppm of Cu Catalyst, $M_n = 18\,300$ g/mol, PDI = 1.11) and PMA_P (ARGET ATRP with 5 ppm of Cu catalyst, $M_n = 18\,500$ g/mol, PDI = 1.77). Panel b: GPC traces after each step of synthesis of block copolymer PS−PMA with different PDI of PMA blocks. Top curve is $(PS\text{-}PMA)_{NP}$ (ARGET ATRP of MA with 5 ppm of Cu catalyst, $M_n = 51\,700$ g/mol, PDI = 1.13). Middle curve is $(PS\text{-}PMA)_{NN}$ (ARGET ATRP of MA with 50 ppm of Cu catalyst, $M_n = 47\,200$ g/mol, PDI = 1.11). Bottom curve is narrow disperse PS macroinitiator (ARGET ATRP of St with 50 ppm of Cu catalyst, $M_n = 31\,100$ g/mol, PDI = 1.11). All molecular weights based on linear PS standards. Panel c: liquid chromatography under critical conditions (LCCC) using critical conditions for PS for $(PS-PMA)_{NP}$ (top curve), $(PS-PMA)_{NN}$ (middle curve), and PS macroinitiator (bottom curve). The LCCC traces indicate 4% PS homopolymer residual for $(PS-PMA)_{NN}$ and 7% PS homopolymer for $(PS-PMA)_{NP}$.

monomer volume and statistical segment lengths: $v_{PS} = 0.98$ nm^3, $v_{PMA} = 0.71$ nm^3, $l_{PS} = 1.1$ nm, $l_{PMA} = 1.4$ nm; with v_i and l_i representing the monomer volume and statistical segment length of polymer i) that is not expected to significantly affect the microphase separation process.[36] Estimating the Flory−Huggins interaction parameter for the PS−PMA system is difficult due to the spread of literature values for the solubility parameters of PS and PMA, i.e., $\delta_{PS} = 17.4-19.0$ MPa$^{0.5}$ and $\delta_{PMA} = 19.9-21.3$ MPa$^{0.5}$. If average values for the solubility parameters are assumed, i.e., $\delta_{PS} = 18.2$ MPa$^{0.5}$ and $\delta_{PMA} = 20.6$ MPa$^{0.5}$, then $\chi_{PS/PMA} = (v_{PS}v_{PMA})^{1/2}(RT)^{-1}(\delta_{PS} - \delta_{PMA})^2$, where R is the gas constant and T is the temperature, yields $N\chi_{PS/PMA}$ well

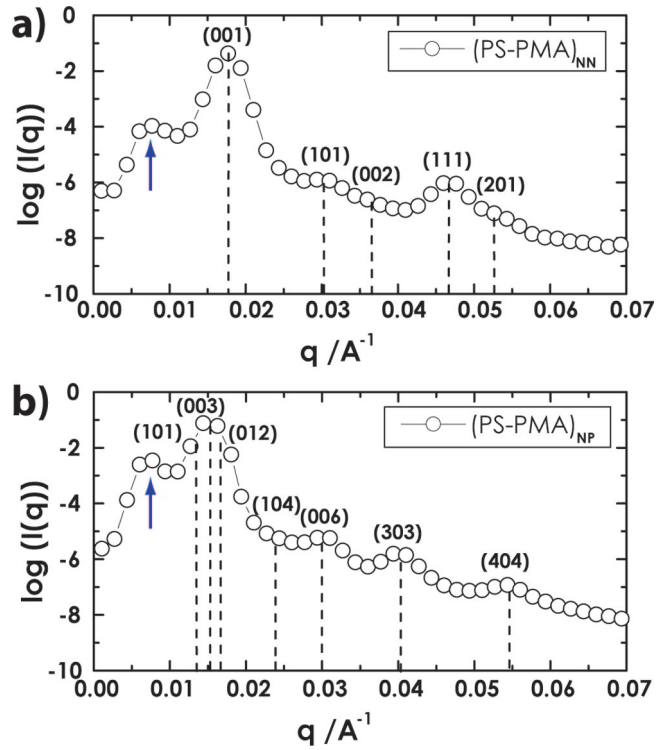

Figure 2. SAXS intensity profiles of $(PS-PMA)_{NN}$ (panel a) and $(PS-PMA)_{NP}$ (panel b) after 72 h thermal annealing at $T = 120$ °C. Vertical lines indicate expected lattice structure factor peaks calculated assuming a *C* microstructure (space group *P6mm*) for $(PS-PMA)_{NN}$ and *HPL* microstructure (space group $R\bar{3}m$) for $(PS-PMA)_{NP}$. Planes are indexed above the peak positions (in standard three index notation). Arrows indicate beamstop position.

above 100 at $T = 298$ K, thus suggesting that both systems are in the strong segregation regime.[37]

Films of both samples were prepared from 10% (w/v) toluene solutions by solvent evaporation (6 days) followed by thermal annealing at $T = 120$ °C (3 days) and analyzed by small-angle X-ray scattering (SAXS) and electron microscopy (TEM). The SAXS intensity profiles obtained from $(PS-PMA)_{NN}$ and $(PS-PMA)_{NP}$ are depicted in Figure 2.

All reflections of the narrow-disperse sample $(PS-PMA)_{NN}$ (see Figure 2a) can be indexed assuming cylindrical morphology (space group *P6mm*). The *C* microstructure is furthermore supported by the electron micrograph shown in Figure 3a and confirms previous studies on the morphology of narrow-disperse PS−PMA copolymers.[38] In contrast, the SAXS pattern of $(PS-PMA)_{NP}$ depicted in Figure 2b can be rationalized assuming a hexagonally perforated lamellar microstructure with space group $R\bar{3}m$. Following this interpretation, the first broad reflection peak at $q = 0.015$ Å^{-1} results from the superposition of the (101), (003), and (012) reflections that cannot be individually resolved using our experimental setup (but note that a shoulder corresponding to the (012) reflection is visible). Assuming the first peak maximum to correspond to the strongest (003) reflection, the hexagonal basis vector length and repeat distance normal to the layer direction follow to be $a = 56.9$ nm and $c = 122.5$ nm, respectively. The $c/a = 2.15$ ratio is similar to that reported previously in *HPL* systems and less than $c/a = 2.45$ that would be expected for a cubic close-packed arrangement of *ABC*-stacked perforations.[39−41] Support for the *HPL* structure is provided by electron micrographs such as Figure 3b (upper left inset) which depicts an area view of a section cut normal to the lamellar orientation, revealing the perforations (bright) within the PMA layers (dark). The absence of the [100] perspective of a cylindrical microstructure among

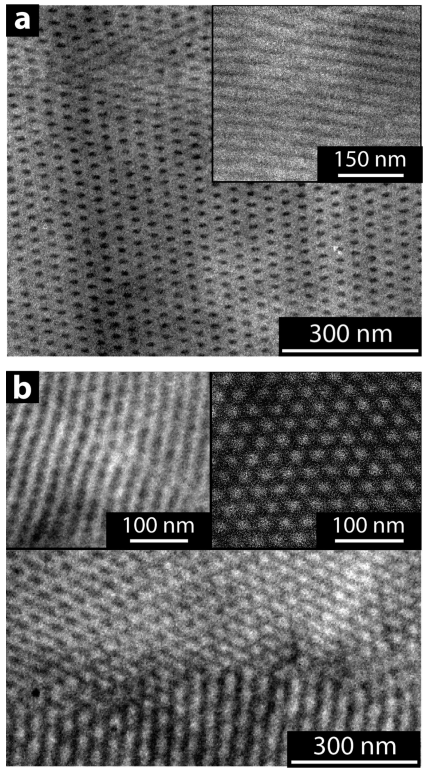

Figure 3. Bright field electron micrographs of PS−PMA samples after 72 h of thermal annealing at $T = 120$ °C and staining with RuO_4 (PMA is dark domain). Panel a: $(PS-PMA)_{NN}$: revealing *C* microstructure imaged along [001] direction. Inset depicts view along [100] direction. Panel b: $(PS-PMA)_{NP}$: revealing *HPL* microstructure imaged at low magnification. The inset on the left depicts the PS-perforations within the PMA layers. The inset on the right shows a plane view revealing the hexagonal arrangement of the PS perforations.

83 micrographs of $(PS–PMA)_{NP}$ provides strong evidence against the existence of alternative structures such as *C* or $L + C$ coexistence. The hexagonal arrangement of the PS perforations is clearly visible in the upper right inset of Figure 3b which depicts a plane view of the PMA layer. The relative positions of the perforations shown in Figure 3b furthermore indicate the *ABC* stacking of the PMA layers that is characteristic for the rhombohedral structure (we note, however, that from the limited TEM data the stacking order of perforations cannot be discerned with absolute certainity). This supports earlier observations of the *HPL* morphology that reported predominantly *ABC* stacking as well as self-consistent-field simulations that suggest the rhombohedral *HPL* structure to be the dominant perforated lamellar structure for degrees of segregation $\chi N > 14$.[42] Figure 4 illustrates the proposed *HPL* microstructure of $(PS-PMA)_{NP}$.

In order to assess the stability of the *HPL* structure in the $(PS-PMA)_{NP}$ system, a series of six film samples were prepared using different processing pathways ranging from 6 days of solvent evaporation and 3 days thermal annealing at $T = 120$ °C to 60 days of solvent evaporation and subsequent thermal annealing at $T = 160$ °C for 3 days. Care was taken to ensure constant solvent evaporation rates in order to avoid the formation of stresses that could interfere with the microdomain ordering. The different sample preparation procedures are summarized in Table 1.

Table 1. Summary of Film Preparation Procedures for $(PS-PMA)_{NP}$ Samples A−E

	preparation path	
sample ID	casting time (days)	thermal history
$(PS-PMA)_{NP}$-A	6	3 days at 120 °C
$(PS-PMA)_{NP}$-B	6	7 days at 120 °C
$(PS-PMA)_{NP}$-C	6	3 days at 120 °C, 4 days at 170 °C
$(PS-PMA)_{NP}$-D	60	none
$(PS-PMA)_{NP}$-E	60	3 days at 160 °C

Figure 5 depicts the near-identical positions of SAXS reflections of samples $(PS-PMA)_{NP}$-A−E, confirming that the *HPL* morphology is attained independent of the processing pathway. For sample $(PS-PMA)_{NP}$-E (60 days solvent evaporation + 3 days thermal annealing at $T = 160$ °C) several additional higher order peaks could be resolved and attributed to the *HPL* structure (not shown here).

Assuming that the slow solvent evaporation and long thermal annealing conditions provide a sufficiently mobile environment for the chains during the microphase separation process to select a low-energy state, we conclude that the observed *HPL* morphology presents a very favorable metastable state or even equilibrium state for the $(PS-PMA)_{NP}$ system. The stability of the *HPL* structure even after months of solvent evaporation and subsequent thermal annealing suggests qualitative differences to narrow-disperse block copolymer systems, for which the role of the *HPL* structure has been the subject of much debate since its first reports.[44] For example, Hajduk et al. demonstrated for several narrow-disperse block copolymer systems that the *HPL* morphology is metastable with respect to the gyroid (*G*).[45] This is in agreement with simulations by Matsen et al., who interpreted the *HPL* structure as a long-lived metastable state at the *L*/*G* boundary.[26] In contrast to the $(PS-PMA)_{NP}$ system, most *HPL* structures reported in the literature were found to be only poorly ordered (Loo et al. interpreted this as an indicator of the metastable nature of the *HPL* structure), typically requiring large-amplitude shear fields for the formation of regular structures.[39] An exception is a recent study by Lai et al., who reported a transition from *L* to a highly regular *HPL* structure in low-molecular-weight PS−PEP at elevated temperatures.[40] In order to elucidate the stability of the *HPL* structure with respect to temperature changes, SAXS data were obtained at $T = 100$, 120, 150, 200, 230, and 300 °C. For each temperature a heating rate of $dT/dt = 10$ °C/min was used, and

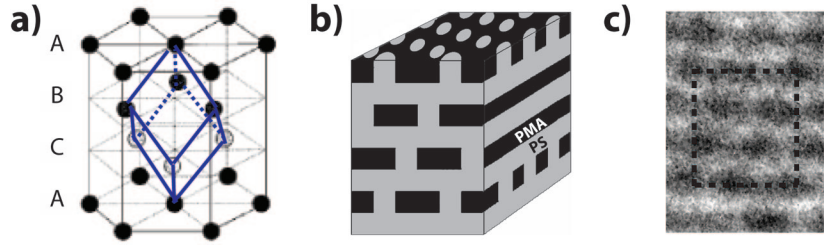

Figure 4. Illustration of the proposed *HPL* microstructure (space group $R\bar{3}m$): Panel a: "ball−stick" model of a rhombohedral unit cell (marked in blue) within an *ABC*-stacked arrangement of spheres. Note that for a close packing of spheres the rhombohedral lattice becomes equivalent to the FCC lattice (space group $F\bar{4}3m$). Panel b: model of the proposed *HPL* microstructure of $(PS-PMA)_{NP}$ (symmetry equivalent to structure shown in panel a) indicating *ABC* stacking of perforations (PS, bright). Panel c: electron micrograph of $(PS-PMA)_{NP}$ (imaged normal to layer direction) revealing the *ABC* stacking of PS perforations (PS, bright).

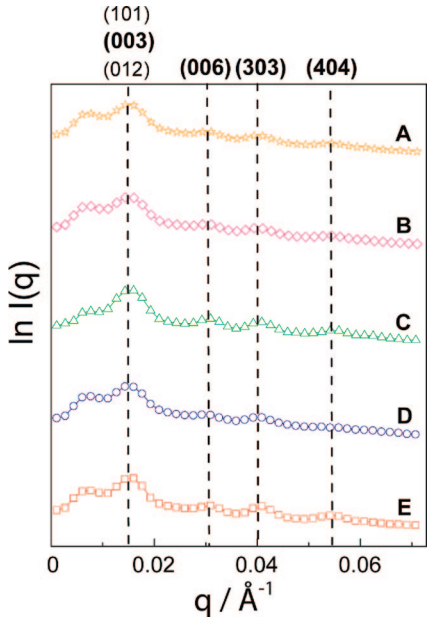

Figure 5. SAXS intensity profiles of $(PS-PMA)_{NP}$ samples A−E that correspond to different sample preparation pathways ranging from 6 days solvent evaporation and 3 days thermal annealing at $T = 120$ °C (sample A) to 60 days solvent evaporation and 3 days thermal annealing at $T = 160$ °C (sample E). Details on the sample processing history are listed in Table 1. Vertical lines indicate expected lattice structure factor peaks for *HPL* microstructure (space group $R\bar{3}m$), and reflections are indexed in standard three index notation. *HPL* morphology is observed for all processing pathways indicating stability of the structure. $q = 0.0075$ Å^{-1} is beamstop position.

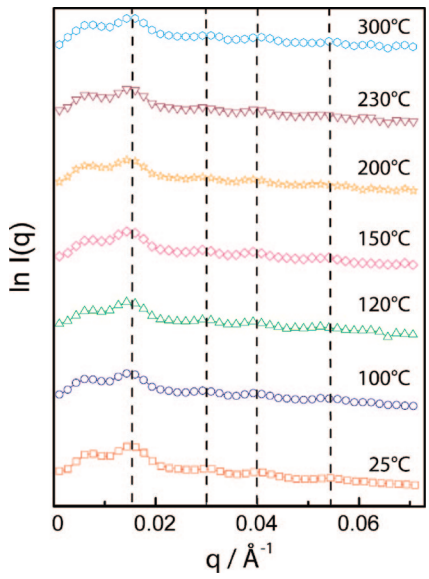

Figure 6. *T*-dependent SAXS intensity profiles of $(PS-PMA)_{NP}$-A measured at $T = 25$, 100, 120, 150, 200, 230, and 300 °C. The heating rate was $dT/dt = 10$ °C/min, and samples were equilibrated for 60 min prior to measurement. For $T = 300$ °C, the sample was allowed to equilibrate for an additional 15 h before measurement. Peak positions remain unchanged, indicating the absence of order−order transitions in the *HPL* microstructure. $q = 0.0075$ Å^{-1} is beamstop position.

the sample was allowed to equilibrate for 60 min. For $T = 300$ °C, the sample was allowed to equilibrate for an additional 15 h. As depicted in Figure 6, no order−order transition was observed at any temperature.

Although the independence of processing pathways as well as *T*-stability do not provide a definite proof of the equilibrium nature of the observed *HPL* structure (for example, a kinetic effect due to the chain dynamics that is expected to be slow because of the rather high molecular weight cannot be completely ruled out), it clearly indicates the extraordinary stabilization of a morphology that is considered to be metastable for narrow-disperse block copolymers. This is also in contrast to previous theoretical studies that conclude the *HPL* does not represent a stable morphology in polydisperse block copolymers.[15] Experimental support for the metastable nature has been provided by Hillmyer and co-workers, who recently reported the formation of a *HPL* structure in a narrow *T*-region of block polydisperse PEP−PLA.[42]

Here we provide a qualitative rationale for the observed stabilization of the *HPL* morphology based on the symmetry of the PMA molecular weight distribution and the assertion of Matsen and Bates that the minimum standard deviation from the mean curvature (σ_H) is the critical parameter for the stabilization of the classical BCP morphologies *L*, *C*, *G*, and *S*.[26,46] According to this argument, the chain packing frustration resulting from the larger σ_H is responsible for the destabilization of the *HPL* and double diamond (*D*) morphologies that would be expected on the basis of only the mean curvature (with the *HPL* considered to be "almost stable" at the *L*/*G* phase boundary).[26] We hypothesize that a symmetric distribution of molecular weights (as in the $(PS-PMA)_{NP}$ system) mitigates the chain packing frustration and thus—for appropriate block compositions—stabilizes structures (such as *HPL*) with $\sigma_H > \sigma_H(G)$. This is because a system comprised of chains with variable length will be better to commensurate with morphologies that exhibit variations in the local environment of the chains (as implied by $\sigma_H > 0$) than a system with perfectly uniform chain characteristics. Since the ability to alleviate packing frustration will depend on the abundance of small and large chains, we expect the symmetry of the molecular weight distribution (MWD) to be an important parameter in determining the structure formation. As noted before, previous theoretical studies only considered the positively skewed Schulz−Zimm distribution to represent the molecular weight distribution. The Schulz−Zimm (SZ) distribution (eq 1) is an empirical two-parameter distribution that is often used because of mathematical convenience and because it has shown to provide a realistic representation for the MWD of step-growth polymerizations:

$$p_{SZ}(N) = \frac{1}{\Gamma(\beta)}\alpha^{\beta}N^{\beta-1}\exp[-\alpha N] \quad (1)$$

with N denoting the degree of polymerization, $\Gamma(N)$ is the Gamma function, N_n the number-average degree of polymerization, $\alpha = \beta/N_n$, and the shape parameter $\beta = (PDI - 1)^{-1}$.[47] A key characteristic of the SZ distribution is its positive skewness; i.e., the number-average molecular weight, M_n, is realized by a majority of chains with molecular weight less than M_n and a few chains with $M \gg M_n$. This is conveniently expressed by introducing the dimensionless skewness indices S_N and S_W, where the subscript refers to the MWD being represented by the number or weight fraction of chains with a particular degree of polymerization, respectively.[48] For any MWD S_N and S_W are defined as

$$S_N = \frac{M_z M_w}{M_n^2} - 3\left(\frac{M_w}{M_n}\right) + 2 \quad (2)$$

$$S_W = \frac{M_{z+1} M_z}{M_w^2} - 3\left(\frac{M_z}{M_w}\right) + 2 \quad (3)$$

where M_i denotes the *i*th average of M that is related to the moments of the MWD via $M_i = \int p(M)M^i\, dM / \int p(M)M^{i-1}\, dM$, with $p(M)$ being the number frequency of M and $i = 1$, 2, 3, and 4 for M_n, M_w, M_z, and M_{z+1}. For a symmetric distribution, $S_{N/W} = 0$, whereas positive (negative) $S_{N/W}$ indicate a distribution

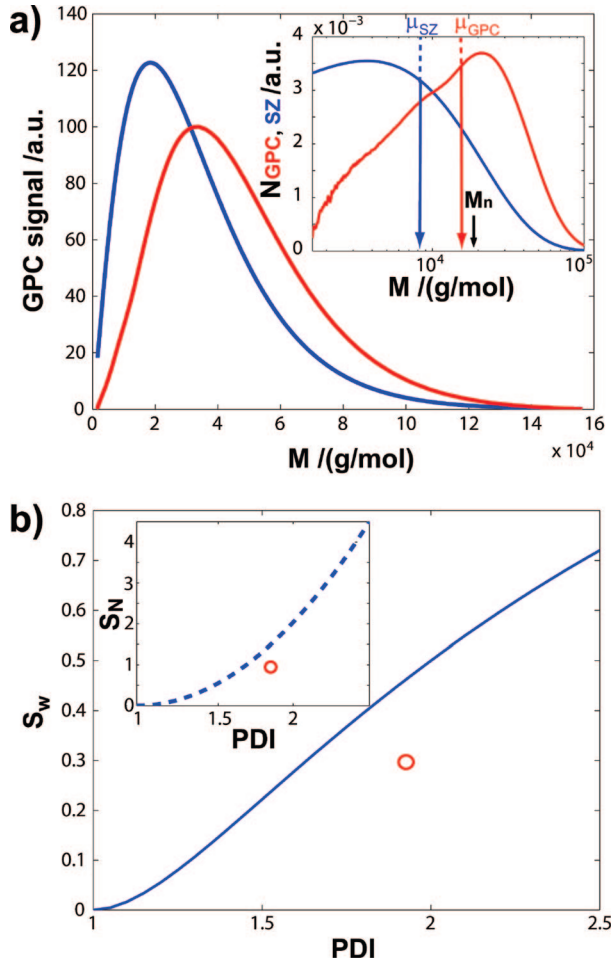

Figure 7. Panel a: plot of the experimental (red) GPC trace of PMA_P homopolymer with M_n = 18 500 g/mol and PDI = 1.77 and the theoretical (blue) GPC trace assuming a SZ distribution for equivalent M_n and PDI calculated using $s_{SZ}(M_i) = M_i N_{SZ}(M_i)$, where s is the GPC signal strength (the GPC signal is mass-weighted due to a light scattering detector) and $N_{SZ}(M_i)$ is the number-weighted SZ MWD given by $N_{SZ}(M_i) = Cp_{SZ}(M)$, where $p_{SZ}(M)$ is the SZ frequency distribution of M (see eq 1), $C = \int N_{GPC}(M)\, dM / \int p_{SZ}(M)\, dM$ is a normalization constant, and $N_{GPC}(M_i)$ is the number-weighted GPC signal (see ref 49). Shown in the inset are the number-weighted MWD as determined by GPC (N_{GPC}, red) and SZ (N_{SZ}, blue). The near-symmetric $N_{GPC}(M_i)$ confirms that the positive skew that is apparent in the GPC data is mostly due to the mass-weighted detection of chains via light scattering. "μ" indicates the position of the median, i.e., the M value separating equal numbers of molecules with M less than or greater than μ (note that for the SZ distribution $\mu_{SZ} \ll M_n$, indicating positive skew). Panel b: plot of mass-weighted skewness index S_W for SZ distribution (blue line) and PMA homopolymer (red circle). $S_{W,SZ} > S_{W,GPC}$ indicates a more symmetric MWD for PMA homopolymer than predicted by the SZ MWD. Inset shows number-weighted skewness index S_N for SZ MWD as well as calculated from GPC data.

skewed toward large (small) M, respectively. Typically, the various molecular weight averages can approximately be determined using GPC. Thus, in order to assess the applicability of the SZ distribution to represent the MWD of the polydisperse PMA block a GPC analysis was performed on a reference polydisperse PMA homopolymer that was synthesized using ARGET ATRP following analogous procedures. Figure 7a compares the experimental GPC trace of the PMA homopolymer with M_n = 18500 g/mol and PDI = 1.77 with the theoretical GPC trace assuming a SZ distribution for equivalent M_n and PDI. The comparison of the number-weighted MWD (shown in the inset of Figure 7a) reveals that the peak of the experimental MWD occurs at approximately $M \approx M_n$, whereas the SZ MWD is peaked at $M \approx 0.3M_n$, indicating a more

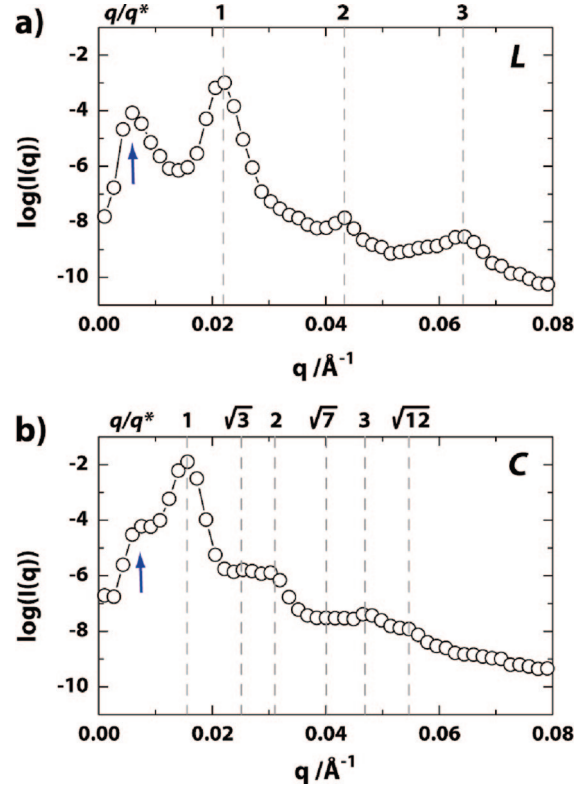

Figure 8. SAXS intensity profiles of PMA−PS copolymers with near-symmetric composition having molecular weights of the MA and S block of MA/S M_n = 17 500/24 500 g/mol (1.15) with total PDI = 1.10 ($(PMA-PS)^*_{NN}$, panel a) and M_n = 25 000/26 000 g/mol (1.55) with total PDI = 1.20 ($(PMA-PS)^*_{PN}$, panel b) where the numbers in parentheses indicate the PDI of the MA block. These samples underwent 6 days of solvent casting and 168 h of thermal annealing at T = 120 °C. Vertical lines indicate expected lattice structure factor peaks calculated assuming (a) a L microstructure (space group Pm) and (b) a C microstructure (space group $P6mm$). The results confirm the $L \rightarrow C$ transition as the PDI of the MA block is increased. Arrows indicate beamstop position.

symmetric MWD for PMA prepared by ARGET ATRP than predicted by SZ.[49] This is confirmed by evaluating the skewness index S_W for PMA (see Figure 7b) that is found to be $S_{W,PMA}$ = 0.29 ($S_{N,PMA}$ = 1.12), significantly below the SZ expectation value of $S_{W,SZ}$ = 0.42 ($S_{N,SZ}$ = 1.18). Note that the mass-weighted skewness index S_W is considered to be more relevant because the microphase separation process depends on the volume fraction of the respective polymer components.

It is conceivable that a system with balanced numbers of small and large chains will be more effective in alleviating packing frustration than a system with strongly skewed MWD and thus be able to stabilize nonregular block copolymer morphologies (a similar argument has been proposed by Pernot et al., who demonstrated the stabilization of bicontinuous blend morphologies by polydisperse graft copolymer surfactants).[50] We expect the implications of the shape of the molecular weight distribution on the structure formation process to be rather subtle and probably most distinguished in narrow compositional regions that correspond to morphologies with relatively large σ_H. This is supported by very recent numerical simulations by Matsen and Hillmyer which suggest that the main influence of the shape of MWD is on the domain spacing rather than the equilibrium morphology (however, these simulations also considered positively skewed distributions with $S_w \approx S_{w,SZ}$).[51] In order to further assess the relevance of the symmetry of the block MWD, the microstructure formation of a PS−PMA copolymer with nearly symmetric composition having comparable total molecular weight to $(PS-PMA)_{NN}$ and $(PS-PMA)_{NP}$ and block-selective

polydispersity in the MA domain was analyzed. Figure 8 presents the SAXS data of two PMA−PS copolymers with molecular weights (in g/mol) of the MA and S block of MA/S M_n = 17 500/24 500 (PDI_{PMA} = 1.15) with total PDI = 1.10 (denoted here as (PMA−PS)*$_{NN}$) and M_n = 25 000/26 000 (PDI_{PMA} = 1.55) with total PDI = 1.20 (denoted here as (PMA−PS)*$_{PN}$), where the numbers in parentheses indicate the PDI in the MA block (for GPC characterization of these polymer samples see Supporting Information, Figure S2).

The peak positions are consistent with a transition $L \rightarrow C$ as the polydispersity of the minority MA domain increases. This is in agreement with theoretical predictions that suggest that the interface between the block domains will bend toward the polydisperse domain and confirms that the fundamental predictions of the impact of block-selective polydispersity are robust with regard to the shape of the molecular weight distribution. An open question remains with respect to the observed *HPL* microstructure in that it occurs for a polydisperse minority component (for which—in principle—a cylindrical or perhaps even spherical morphology would be expected).[15] We attribute its occurrence to the cumulative effect of composition, molecular weight, symmetric MWD, as well as the presence of residual macroinitiator. Ultimately, the presence of even a minor amount of macroinitiator needs to be considered, since previous studies by Spontak and co-workers revealed that homopolymer additives can stabilize *HPL* microstructures (in the case of block copolymer/homopolymer blends, the *HPL* morphology was denoted catenoid-lamellar); however, the stabilization was reported for volume fractions of homopolymer an order of magnitude larger than the amount of macroinitiator present in (PS−PMA)$_{NP}$.[52] Theoretical studies will be needed to better understand the effect of the symmetry of molecular weight distribution on the microphase separation and structure selection process.

Conclusion

As has been shown previously, the implications of polydispersity of block copolymers and, in particular, its effect on the microphase separation process are of central importance to develop and exploit the potential of new polymerization techniques such as controlled radical polymerization. Next to the PDI itself, the present study suggests that the symmetry of the molecular weight distribution is an important parameter in controlling the structure formation process. The stabilization of the *HPL* morphology in the case of a PS−PMA copolymer with a block polydispersity of the polydisperse MA domain of PDI between 1.5 and 2 is interpreted as a consequence of the efficient alleviation of packing frustration that is facilitated by the balanced presence of small and large chains of the minority component. The $L \rightarrow C$ transition in a compositionally symmetric PS−PMA copolymer indicates that the fundamental predictions of the effect of block-selective polydispersity on the microstructure formation process (that were derived on the basis of skewed molecular weight distributions) are robust with respect to the shape of distributions but that the relative abundance of small and large chains can alter the stabilization of (classically) metastable morphologies. Finally, the results point to the relevance of developing novel synthetic techniques such as ARGET ATRP which facilitate the preparation of block copolymers with varying PDI and near-symmetric molecular weight distributions and thus potentially provide a route toward the targeted synthesis of nonregular microstructures with particular topological characteristics (such as combined 2D/3D continuity in the case of the *HPL* morphology) that might be of future technological interest.

Experimental Section

Materials. Methyl acrylate (MA) (Aldrich, 99%) and styrene (S) (Aldrich, 99%), were passed through a column filled with neutral alumina to remove inhibitor. Tris(2-pyridylmethyl)amine (TPMA)[53] and tris(2-(dimethylamino)ethyl)amine (Me_6TREN)[54] were synthesized following the previously reported procedure. Copper(II) bromide (Acros, 99%), ethyl 2-bromoisobutyrate (EtBrIB) (Acros, 98%), 1-phenylethyl bromide (PEBr) (Aldrich, 97%), tin(II) 2-ethylhexanoate ($Sn(EH)_2$) (Aldrich, 95%), toluene (Aldrich, 99%), and anisole (Aldrich, 99%) were used as received. Copper(I) bromide (Acros, 95%) was washed with glacial acetic acid in order to remove any soluble oxidized species, filtered, washed with ethanol, and dried.

Synthesis of PS Macroinitiator Using ARGET ATRP (Targeting Number-Average Degree of Polymerization (DP_n) of 340), with 50 ppm of Cu. Degassed styrene (10 mL, 87 mmol) was transferred via degassed syringes to a dry Schlenk flask, thoroughly purged by flushing with nitrogen. Next, CuBr (0.63 mg, 0.44×10^{-2} mmol)/Me_6TREN (6.78 μL, 2.57×10^{-2} mmol) complex in degassed anisole (2.0 mL) was added. The resulting mixture was stirred for 10 min, and then a purged solution of $Sn(EH)_2$ (8.33 μL, 2.57×10^{-2} mmol) in anisole (0.5 mL) was added. Then EtBrIB (37.7 μL, 25.7×10^{-2} mmol) initiator in degassed anisole (0.5 mL) was added to initiate the polymerization. An initial sample was taken, and the sealed flask was placed in thermostated oil bath at 100 °C. The polymerization was stopped after 41 h at conversion of 84% ($M_{n,GPC}$ = 31 100 g/mol, PDI = 1.11, after precipitation) by opening the flask and exposing the catalyst to air.

Synthesis of PMA Homopolymers Using ARGET ATRP (Targeting DP_n = 350), with 50 and 5 ppm of Cu. Degassed MA monomer (0.91 mL, 9.77 mmol) and degassed toluene (1 mL—to take place of 1 g of PSt macroinitiator) were transferred via degassed syringes to a dry Schlenk flask, thoroughly purged by flushing with nitrogen. Next, a solution of CuBr (6.98×10^{-2} mg, 0.49×10^{-3} mmol)/TPMA (0.48 mg, 1.67×10^{-3} mmol) complex in degassed anisole (0.5 mL) was added followed by addition of a solution of PEBr (3.8 μL, 2.78×10^{-2} mmol) in anisole (0.4 mL). The resulting mixture was stirred for 10 min, and then a purged solution of $Sn(EH)_2$ (0.9 μL, 2.8×10^{-3} mmol) in anisole (0.1 mL) was added. An initial sample was taken, and the sealed flask was placed in thermostated oil bath at 60 °C. The polymerization was stopped after 44 h ($M_{n,GPC}$ = 18 300 g/mol, PDI = 1.11, conversion = 55%) by opening the flask and exposing the catalyst to air. A similar procedure was used in the synthesis of PMA (polydisperse), but a lower amount of copper catalyst was used (5 ppm amount vs monomer) and Me_6TREN ligand was used instead of TPMA. This polymerization was stopped after 27 h ($M_{n,GPC}$ = 18 500 g/mol, PDI = 1.77, conversion = 56%). The entire samples were analyzed by GPC without any fractionation or precipitation. Subsequently, each polymer was precipitated into hexanes. After precipitation, the narrow disperse PMA had $M_{n,GPC}$ = 17 500 g/mol and PDI = 1.12, and after precipitation of the polydisperse PMA block, $M_{n,GPC}$ = 25 000 g/mol and PDI = 1.55. These copolymers were used as macroinitiators for chain extension with styrene ((PS−PMA)*$_{NN}$ and (PS−PMA)*$_{PN}$).

Synthesis of Diblock Copolymers (PS−PMA)$_{NN}$ and (PS−PMA)$_{NP}$ Using ARGET ATRP (Targeting DP_n = 350), with 50 and 5 ppm of Cu. A PS macroinitiator ($M_{n,GPC}$ = 31 100 g/mol, PDI = 1.11) (1.00 g, 2.78×10^{-2} mmol) was dissolved in MA monomer (0.91 mL, 9.77 mmol) and anisole (0.4 mL) in a 10 mL Schlenk flask and bubbled with nitrogen for 15 min. Next, a solution of CuBr (6.98×10^{-2} mg, 0.49×10^{-3} mmol)/TPMA (0.48 mg, 1.67×10^{-3} mmol) complex in degassed anisole (0.5 mL) was added. The resulting mixture was stirred for 10 min, and then a purged solution of $Sn(EH)_2$ (0.9 μL, 2.8×10^{-3} mmol) in anisole (0.1 mL) was added. An initial sample was taken, and the sealed flask was placed in thermostated oil bath at 60 °C. The polymerization was stopped after 44 h at conversion of 68% ($M_{n,GPC}$ = 47 200 g/mol, PDI = 1.11, after precipitation) by opening the

flask and exposing the catalyst to air. A similar procedure was used in the synthesis of $(PS-PMA)_{NP}$, but a lower amount of copper catalyst was used (5 ppm amount vs monomer) and Me_6TREN ligand was used instead of TPMA; final $M_{n,GPC} = 51\,700$, PDI = 1.13 after precipitation (conversion = 63%). Residual PS macroinitiator was detected by the meaning of LCCC (4 and 7% for $(PS-PMA)_{NP}$ and $(PS-PMA)_{NP}$, respectively).

Synthesis of Diblock Copolymers $(PMA-PS)^*_{NN}$ and $(PMA-PS)^*_{PN}$ Using ARGET ATRP (Targeting $DP_n = 640$), with 50 ppm of Cu. PMA macroinitiator ($M_{n,GPC} = 17\,500$ g/mol and PDI = 1.12) (0.22 g, 1.25×10^{-2} mmol) was dissolved in anisole (1 mL) in a 10 mL Schlenk flask and bubbled with nitrogen for 15 min. Degassed styrene (0.92 mL, 8.03 mmol) was transferred to the flask via a degassed syringe. Next, a solution of $CuBr_2$ (8.90×10^{-2} mg, 0.40×10^{-3} mmol)/TPMA (0.22 mg, 0.76×10^{-3} mmol) complex in degassed anisole (0.5 mL) was added. The resulting mixture was stirred for 10 min, and then a purged solution of $Sn(EH)_2$ (0.4 μL, 1.3×10^{-3} mmol) in anisole (0.5 mL) was added. An initial sample was taken, and the sealed flask was placed in thermostated oil bath at 90 °C. The polymerization was stopped after 50 h ($M_{n,GPC} = 42\,000$ g/mol, PDI = 1.10, conversion = 37%) by opening the flask and exposing the catalyst to air. The same procedure was used to extend PMA macroinitiator ($M_{n,GPC} = 25\,000$ g/mol and PDI = 1.55) (0.31 g, 1.25×10^{-2} mmol) with styrene. After 50 h ($M_{n,GPC} = 51\,000$ g/mol and PDI = 1.20), the polymerization was stopped by opening the flask and exposing the catalyst to air. LCCC traces of these copolymers are available in the Supporting Information, Figure S3.

General Analysis. Molecular weight and polydispersity were determined by GPC, conducted with a Waters 515 pump and a Waters 2414 differential refractometer using PSS columns (Styrogel 10^5, 10^3, and 10^2 Å) in THF as an eluent at 35 °C and at a flow rate of 1 mL/min. Linear polystyrene standards were used for calibration. Monomer conversion was determined using a Shimadzu GC 14-A gas chromatograph equipped with a FID detector using a J&W Scientific 30 m DB WAX Megabore column with anisole as an internal standard. Injector and detector temperatures were kept constant at 250 °C. Analysis was carried out isothermally at 60 °C for 2 min followed by an increase of temperature to 160 °C at a heating rate of 40 °C/min and holding at 160 °C for 2 min. Conversion was calculated by detecting the decrease of the monomer peak area relative to the peak areas of the standards. Liquid chromatography under the critical conditions (LCCC) of PS homopolymer was used to analyze the $(PS-PMA)_{NN}$ and $(PS-PMA)_{NP}$ copolymers by using two sets of Macherey & Nagel Nucleosil normal phase silica columns with pore size of 100 and 300 Å as stationary phase and tetrahydrofuran/acetonitrile (49/51 by volume) as mobile phase (flow rate = 0.5 mL/min, 32 °C). A Waters 600 controller and pump containing a multisolvent delivery system and an evaporative light scattering (ELS) detector (Polymer Laboratories, PLS6 ELS 1000, Amherst, MA, nitrogen flow 1.2 L/min, evaporator temperature 90 °C) were used in all LCCC analyses of the block copolymers. Before injection, the samples were dissolved in tetrahydrofuran/acetonitrile (50/50 by volume) at the concentration of 0.5 mg/mL.

Film Preparation. Block copolymer films of about 1 mm thickness were obtained by casting a 10% polymer solution in toluene (approximately nonpreferential solvent) and slowly evaporating the solvent over a period as specified in the text (see Table 1). The resulting films were thermally annealed under vacuum as described in Table 1. Films were microsectioned at −120 °C using a LEICA EM FCS cryo-ultra microtome. To enhance contrast, microsections were stained using ruthenium tetroxide (obtained from EM Sciences), which preferentially stained the PMA domains.

Transmission Electron Microscopy (TEM). TEM was performed using a JEOL 2000 EX electron microscope operated at 200 kV. Imaging was done by amplitude and phase contrast, and images were acquired using a Gatan Orius SC600 high-resolution camera.

Small-Angle X-ray Scattering (SAXS). SAXS data were acquired under vacuum using a Rigaku S-Max3000 with a 2D multiwire detector equipped with a Linkam LTS 350 hot stage. Two-dimensional SAXS patterns were azimuthally integrated to obtain plots of scattered intensity vs momentum transfer vector, $q = (4\pi/\lambda) \sin\theta$, where θ is half the scattering angle and $\lambda = 1.54$ Å. Peaks were fit with Gaussian functions to determine the locations of the peak maxima.

Acknowledgment. Financial support by the Petroleum Research Fund administered by the American Chemical Society as well as the National Science Foundation (via grants DMR-0706265, DMR-0549353, and CTS-0521079) is gratefully acknowledged. L.M. acknowledges her NSF fellowship. The authors also thank Guy C. Berry for helpful discussions and Haifeng Gao and Wenwen Li for 2D chromatography analysis.

Supporting Information Available: Experimental details. This material is available free of charge via the Internet at http://pubs.acs.org.

References and Notes

(1) Park, C.; Yoon, J.; Thomas, E. L. *Polymer* **2003**, *44*, 6725–6760.
(2) (a) Bockstaller, M. R.; Mickiewicz, R. A.; Thomas, E. L. *Adv. Mater.* **2005**, *17*, 1331–1349. (b) Bockstaller, M. R.; Kolb, R.; Thomas, E. L. *Adv. Mater.* **2001**, *13*, 1783–1786.
(3) Braunecker, W. A.; Matyjaszewski, K. *Prog. Polym. Sci.* **2007**, *32*, 93–146.
(4) Wang, J.-S.; Matyjaszewski, K. *J. Am. Chem. Soc.* **1995**, *117*, 5614–5615.
(5) Kato, M.; Kamigaito, M.; Sawamoto, M.; Higashimura, T. *Macromolecules* **1995**, *28*, 1721–1723.
(6) Matyjaszewski, K.; Xia, J. *Chem. Rev.* **2001**, *101*, 2921–2990.
(7) Hawker, C. J.; Bosman, A. W.; Harth, E. *Chem. Rev.* **2001**, *101*, 3661–3688.
(8) Chiefari, J.; Chong, Y. K.; Ercole, F.; Krstina, J.; Jeffery, J.; Le, T. P.; Mayadunne, R. T.; Meijs, G. F.; Moad, C. L.; Moad, G.; Rizzardo, E.; Thang, S. H. *Macromolecules* **1998**, *31*, 5559–5562.
(9) Leibler, L.; Benoit, H. *Polymer* **1981**, *22*, 195–201.
(10) Hong, K. M.; Noolandi, J. *J. Polym. Commun.* **1984**, *25*, 265–268.
(11) Burger, C.; Ruland, W.; Semenov, A. N. *Macromolecules* **1990**, *23*, 3339–3346.
(12) Sides, W.; Fredrickson, G. H. *J. Chem. Phys.* **2004**, *121*, 4974–4986.
(13) Cooke, D. M.; Shi, A.-C. *Macromolecules* **2006**, *39*, 6661–6671.
(14) Matsen, M. W. *Eur. Phys. J. E* **2006**, *21*, 199–207.
(15) Matsen, M. W. *Phys. Rev. Lett.* **2007**, *99* (148304), 1–4.
(16) Hashimoto, T.; Yamasaki, K.; Koizumi, S.; Hasegawa, H. *Macromolecules* **1993**, *26*, 2895–2904.
(17) Spontak, R. J. *Macromolecules* **1994**, *27*, 6363–6370.
(18) Court, F.; Hashimoto, T. *Macromolecules* **2001**, *34*, 2536–2545.
(19) Court, F.; Hashimoto, T. *Macromolecules* **2002**, *35*, 2566–2575.
(20) Matsushita, Y.; Noro, A.; Iinuma, M.; Suzuki, J.; Ohtani, H.; Takano, A. *Macromolecules* **2003**, *36*, 8074–8077.
(21) Noro, A.; Iinuma, M.; Suzuki, J.; Takano, A.; Matsushita, Y. *Macromolecules* **2004**, *37*, 3804–3808.
(22) Hashimoto, T.; Tanaka, H.; Hasegawa, H. *Macromolecules* **1985**, *18*, 1864.
(23) Bendejacq, D.; Ponsinet, V.; Joanicot, M.; Loo, Y.-L.; Register, R. A. *Macromolecules* **2002**, *35*, 6645–6649.
(24) Lynd, N. A.; Hillmyer, M. A. *Macromolecules* **2005**, *38*, 8803–8810.
(25) Ruzette, A.-V.; Tence-Girault, S.; Leibler, L.; Chauvin, F.; Bertin, D.; Guerret, O.; Gerard, P. *Macromolecules* **2006**, *39*, 5804–5814.
(26) (a) Matsen, M. W.; Bates, F. S. *Macromolecules* **1996**, *29*, 1091–1098. (b) Matsen, M. W.; Bates, F. S. *Macromolecules* **1996**, *29*, 7641–7644.
(27) Jakubowski, W.; Min, K.; Matyjaszewski, K. *Macromolecules* **2006**, *39*, 39–45.
(28) Matyjaszewski, K.; Jakubowski, W.; Min, K.; Tang, W.; Huang, J. Y.; Braunecker, W. A.; Tsarevsky, N. V. *Proc. Natl. Acad. Sci. U.S.A.* **2006**, *103*, 15309–15314.
(29) Tsarevsky, N. V.; Bencherif, S. A.; Matyjaszewski, K. *Macromolecules* **2007**, *40*, 4439–4445.
(30) Min, K.; Gao, H.; Matyjaszewski, K. *Macromolecules* **2007**, *40*, 1789–1791.
(31) Dong, H.; Tang, W.; Matyjaszewski, K. *Macromolecules* **2007**, *402974*–2977.
(32) Pietrasik, J.; Dong, H.; Matyjaszewski, K. *Macromolecules* **2006**, *39*, 6384–6390.
(33) Matyjaszewski, K.; Dong, H.; Jakubowski, W.; Pietrasik, J.; Kusumo, A. *Langmuir* **2007**, *23*, 4528–4531.

(34) Jakubowski, W.; Matyjaszewski, K. *Angew. Chem., Int. Ed.* **2006**, *45*, 4482–4486.
(35) The conversion of retention volume to molecular weight yields a weakly skewed distribution characterized by a Pearson skewness coefficient $\kappa \approx -0.2$. This skewness parameter is considered to be negligible compared to the respective Schulz−Zimm distribution ($\kappa \approx -1.1$).
(36) Brandrup, J., Immergut, E. H., Grulke, H., Eds. *Polymer Handbook*; John Wiley & Sons: New York, 2003.
(37) Van Krevelen, D. W.; Hoftyzer, P. J. *Properties of Polymers. Correlations with Chemical Structure*; Elsevier: New York, 1972.
(38) Anand, P. S.; Stahl, H. G.; Heitz, W.; Weber, G.; Bottenbruch, L. *Makromol. Chem.* **2003**, *183*, 1685–1700.
(39) Loo, Y.-L.; Register, R. A.; Adamson, D. H.; Ryan, A. J. *Macromolecules* **2005**, *38*, 4947–4949.
(40) Lai, C.; Loo, Y.-L.; Register, R. A.; Adamson, D. H. *Macromolecules* **2005**, *38*, 7098.
(41) Ahn, J.-H.; Zin, W.-C. *Macromolecues* **2000**, *33*, 641–644.
(42) Lynd, N. A.; Hillmyer, M. A. *Macromolecules* **2007**, *40*, 8050–8055.
(43) Matsen, M. W. *Phys. Rev. Lett.* **1998**, *80*, 201.
(44) (a) Hashimoto, T.; Koizumi, S.; Hasegawa, H.; Izumitani, T.; Hyde, S. T. *Macromolecules* **1992**, *25*, 1433–1439. (b) Almdal, K.; Koppi, K. A.; Bates, F. S.; Mortensen, K. *Macromolecules* **1992**, *25*, 1743–1751. (c) Spontak, R. J.; Smith, S. D.; Ashraf, A. *Macromolecules* **1993**, *26*, 956–962.
(45) Hajduk, D. A.; Takenouchi, H.; Hillmyer, M. A.; Bates, F. S.; Vigild, M. E.; Almdal, K. *Macromolecules* **1997**, *30*, 3788–3795.
(46) The interpretation of the relevance of σ_H originally given by Matsen and Bates was based on the evaluation of intermaterial dividing surfaces that were calculated at the *C*/*G* boundary for $\chi N = 20$, $\phi = 0.3378$. Minor deviations in the actual numbers can be expected for the composition of $(PS-PMA)_{NP}$ since $\phi_{MA} \sim 0.35$.
(47) Strobl, G. *The Physics of Polymers*, 3rd ed.; Springer: Berlin, 2007.
(48) Berry, G. C. Polymer Molecular Weight and its Distribution. In *Encyclopedia of Materials: Science and Technology*; Elsevier: New York, 2001.
(49) The number-weighted GPC signal can be deduced from the experimental GPC trace (determined using light scattering) by $N_{GPC}(M_i) = s_i(M_i)/M_i$, where $s_i(M_i)$ denotes the detector signal for chains with molecular weight M_i.
(50) Pernot, H.; Baumert, M.; Court, F.; Leibler, L. *Nat. Mater.* **2002**, *1*, 54–58.
(51) Matsen, M., private conversation.
(52) Spontak, R. J.; Smith, S. D.; Asharaf, A. *Macromolecules* **1993**, *26*, 956.
(53) (a) Tyeklar, Z.; Jacobson, R. R.; Wei, N.; Murthy, N. N.; Zubieta, J.; Karlin, K. D. *J. Am. Chem. Soc.* **1993**, *115*, 2677. (b) Xia, J.; Matyjaszewski, K. *Macromolecules* **1999**, *32*, 2434–2437.
(54) Xia, J.; Gaynor, S. G.; Matyjaszewski, K. *Macromolecules* **1998**, *31*, 5958–5959.

MA800816J